Acta Materialia 297 (2025) 121347

Contents lists available at ScienceDirect

Acta Materialia

journal homepage: www.elsevier.com/locate/actamat

Full length article

Machine learning-driven discovery of hard magnetic materials using high-throughput computation and screening

Anita Halder [a,b], Durga Paudyal [c], Stefano Sanvito [a], Martin Takáč [d], Huseyin Ucar [d,e,*]

[a] School of Physics, AMBER and CRANN Institute, Trinity College Dublin, Dublin 2, Dublin, D02 W085, Ireland
[b] Department of Physics and Centre for Computational and Integrative Sciences, SRM University-AP, Mangalagiri, Amravati, 522240, Andhra Pradesh, India
[c] Department of Physics and Astronomy, University of Iowa, Iowa City, 52242, IA, USA
[d] Machine Learning Department, Mohamed bin Zayed University of Artificial Intelligence (MBZUAI), Masdar City, Abu Dhabi, United Arab Emirates
[e] Chemical and Materials Engineering Department, California Polytechnic University, 3801 West Temple Avenue, Pomona, 91768, CA, USA

ARTICLE INFO

Keywords:
Permanent magnets
FeCo-based alloys
Magnetocrystalline anisotropy energy
Curie temperature prediction
High-throughput materials discovery

ABSTRACT

We present a machine-learning-driven framework for discovering high-performance rare-earth-free hard magnetic materials integrating machine learning, a universal graph deep-learning interatomic potential, and density functional theory validation. Key contributions include the identification of FeCo-based ternary alloys with remarkable magnetic properties, such as uniaxial anisotropy constant, K_1, Curie temperature, T_C, and saturation magnetization, M_S. Notable examples include Fe_6CoB_2 and $FeCo_5B$, which exhibit K_1 values of 1.76 MJ/m^3 and 1.00 MJ/m^3, respectively, with M_S above 1.3 T, and T_C exceeding 600 K. These properties align with the needs of high-temperature and high-performance applications. The universal graph deep-learning interatomic potential M3GNet accelerates the structural relaxation process, enabling the efficient screening of 48,000 candidate structures, while density functional theory validates the top performers with energy product $(BH)_{max}$ reaching more than 600 kJ/m^3. Our study highlights a scalable, efficient pipeline for advancing the discovery of permanent magnets, reducing reliance on rare-earth elements.

1. Introduction

Magnetic materials are integral to modern technological advancements, driving significant research and development efforts to enhance their performance, efficiency and cost-effectiveness. Permanent magnets serve as foundational components in various applications, including traction motors, loudspeakers, wind turbines, magnetic refrigeration, and cancer thermotherapy [1,2]. Despite their crucial role, the traditional trial-and-error approach to materials discovery remains slow and costly, often requiring decades for new materials to transition from laboratory research to commercial applications [3].

Recent shifts toward computational materials discovery, enabled by supercomputers and first-principles physics, offer promising alternatives. Large-scale computational infrastructures can now determine the ground state of solid-state inorganic crystals in a high-throughput manner within the framework of Density Functional Theory (DFT). This approach significantly accelerates the discovery process, reducing the time and cost associated with experimental trials [4].

Databases such as the Open Quantum Materials Database (OQMD) [5], the Automatic Flow of Materials Discovery Library (AFLOWLIB) [6], and the Materials Project (MP) [7] provide extensive repositories of thermodynamic and electronic properties. However, key magnetic properties, such as the magnetocrystalline anisotropy energy (MCA), and the Curie temperature (T_C), are underrepresented in these repositories. This is due to the high computational costs associated to their calculation [8,9]. For example, the MCA is an intrinsic relativistic phenomenon arising from spin–orbit coupling (SOC), and typically involves the evaluation of tiny energy differences [10]. Similarly, computing T_C is a complex process, where one typically maps DFT total-energy calculations onto a Heisenberg-type model and then either performs Monte Carlo simulations or evaluates mean field theory (MFT) expressions [11]. Moreover, magnetism is often governed by electrons in the localized *4f* and *3d* shells, a fact that pose challenges to standard DFT methodologies. These limitations are addressed using auxiliary methods such as DFT+Hubbard-*U* [12,13] or the integration of dynamical mean field theory (DMFT) [14]. While these approaches improve the accuracy of the predictions of magnetic properties, they are computationally prohibitive for high-throughput workflows, creating a bottleneck for

* Corresponding author at: Chemical and Materials Engineering Department, California Polytechnic University, 3801 West Temple Avenue, Pomona, 91768, CA, USA.
E-mail address: hucar@cpp.edu (H. Ucar).

https://doi.org/10.1016/j.actamat.2025.121347
Received 13 February 2025; Received in revised form 7 July 2025; Accepted 15 July 2025
Available online 28 July 2025

generating the high-fidelity datasets required for developing robust machine-learning (ML) models.

For materials with a simpler electronic structure and spin arrangement, a discovery workflow combining high-throughput computational approaches with ML has shown considerable promise in identifying new magnetic compounds. For instance, Sanvito et al. used DFT to generate a large database of magnetic properties of Heusler alloys, and trained a ML model to evaluate their T_C. This enabled the discovery of a novel high-T_C ferromagnet, Co_2MnTi, and a complex antiferromagnet, Mn_2PtPd, then synthesized in the lab [15]. Halder et al. employed DFT and ML models to predict and optimize the magnetic properties, stability, and efficiency of rare-earth-lean magnets. They demonstrated that $Ce_2Fe_{17-x}Co_xCN$ offers potential to be a cost-effective and high-performance permanent magnet [16]. Xia et al. developed a machine-learning-guided adaptive genetic algorithm in conjunction with a crystal-graph convolutional neural network (CGCNN) to efficiently screen Fe-Co-B compounds as high-performance, rare-earth-free, magnetic materials. Their approach involved training a ML model on DFT-calculated structures to predict formation energies, which in turn enabled the selection of stable Fe-Co-B systems with large magnetocrystalline anisotropy and high Curie temperatures. Notably, they also synthesized Fe_3CoB_2, which was confirmed to display strong magnetic properties, including $K_1 \approx 1.2\,\mathrm{MJ/m^3}$ and $J_s \approx 1.4\,\mathrm{T}$. The enhanced anisotropy was attributed to the boron incorporation into the Fe-Co matrix. [17]. In another study, Xia et al. [18] developed a machine-learning-guided framework, combining CGCNN and an adaptive genetic algorithm, to discover Fe-Co-C ternary compounds with high magnetic anisotropy. In particular, they, identified five metastable and dynamically stable candidates with $K_1 > 1.0\,\mathrm{MJ/m^3}$, $J_s > 1.0\,\mathrm{T}$, and $T_c > 840\,\mathrm{K}$. Liao et al. conducted a machine-learning-accelerated search across the Fe-Co-P ternary space, identifying 16 new structures below the convex hull, including five with $J_s > 1$ T and promising anisotropy, with Fe_7CoP_4 emerging as the top candidate ($J_s = 1.03$ T, $K_1 = 0.83\,\mathrm{MJ/m^3}$) as a rare-earth-free permanent magnet [19].

We also acknowledge recent related works by Schmidt et al. [20] and Vishina et al. [21], which offer complementary machine-learning and experimental perspectives on the discovery of rare-earth-free magnetic materials. Schmidt et al. developed a crystal graph attention network (CGAT) capable of predicting thermodynamic stability (distance to convex hull) without requiring fully relaxed crystal structures. By combining prototype-based modeling with attention-based message passing, their approach enables high-throughput discovery of stable compounds across millions of hypothetical compositions. Vishina et al. proposed a new class of rare-earth-free permanent magnets based on the Co_3Mn_2Ge compound, identified through high-throughput data mining and validated experimentally. Lastly, Horton et al. developed a framework that predicts the magnetic ground state of crystals (ferromagnetic, antiferromagnetic, or ferrimagnetic) and their associated magnetic moments using collinear spin-polarized DFT in a high-throughput manner, achieving around 60% accuracy on experimental datasets [22].

In this work, we present a pipeline for the discovery of permanent magnets that generates ternary magnetic alloys and predicts their key hard magnetic properties, including easy axis anisotropy (K_1), magnetic transition temperature (T_C), and saturation magnetization (M_S). Our methodology involves three main steps. Firstly, regression ML models are trained to predict M_S and T_C, while a classification ML algorithm predicts whether a structure is likely to exhibit an easy magnetization axis. These are all based on structural features. The classifier serves as a screening tool to select materials that are likely to exhibit easy axis anisotropy as opposed to easy plane one. Secondly, new structures are generated by substituting Fe and Co at transition-metal (TM) sites and boron or nitrogen at non-TM sites within ternary alloys sourced from the AFLOW repository. Structural relaxation is performed using the M3GNet universal potential [23]. Finally, the trained ML models predict the key magnetic properties of these structures, and the top candidates are then selected based on their magnetic properties and structural stability against decomposition. The properties of these candidates are subsequently evaluated via DFT.

In particular, we aim at developing rare-earth-free permanent magnets, considering the limited availability and supply-chain vulnerabilities of rare-earth resources. The choice of elements in our approach is deliberate: Fe is used for its role in providing high M_S, Co contributes significantly to the MCA, and elements such as nitrogen and carbon enhance the structural stability and may increase T_C [10,24,25]. Our multipronged strategy allows for the exploration of diverse compositions and helps to determine the optimal compositional ratios necessary to achieve the desired combination of magnetic properties and stability. This approach is critical for designing sustainable and high-performance permanent magnets. The overall framework is illustrated in Fig. 1.

The key contributions of this paper are as follows: (1) the use of robust ML models to predict critical magnetic properties, enabling scalable screening of structures; (2) the application of M3GNet graph neural networks to accelerate structural relaxations, reducing computational demands compared to DFT; and (3) the rigorous validation of top-performing, structurally stable materials using DFT.

2. Methods

2.1. Dataset generation

The first stage of our materials discovery pipeline involves curating three separate datasets for training the ML models. These models are designed to predict (i) M_S, (ii) T_C, and (iii) the easy axis anisotropy. Magnetic moment data and corresponding structures for approximately 150,000 compounds were downloaded using the Materials Project (MP) API. This data was used to train the magnetic moment regressor using the universal-graph deep-learning architecture M3GNet [23].

Although there are T_C datasets that are generated using natural language processing methods [26], their accuracy still could not achieve to those developed manually. Therefore, we began with the T_C dataset manually compiled as used in Gilligan et al. [27], which consists of approximately 5400 compounds with compositions and corresponding T_C values. Since we aimed to train a T_C model using structural information, we obtained the structures for these compositions from the MP [7] and AFLOW [6] APIs. These databases often contain multiple structures for the same composition due to polymorphs or hypothetical structures analyzed for stability. For each composition, only the stable structures on the convex hull were retrieved, which refer to the crystal structures that are thermodynamically stable with respect to decomposition into competing phases. These structures lie on the convex hull constructed with the formation energies of all known phases at a given composition. Only the lowest-energy structures that define this convex envelope are considered stable. Out of the 5400 compounds, approximately 1500 records met this requirement. We acknowledge that T_C can differ across different polymorphs of the same composition. However, our T_C dataset is experimentally derived and lacks explicit structural information. Therefore, to associate each composition with a physically meaningful structure, we retrieved only the lowest-energy phase on the convex hull from DFT-based databases. These structures are more likely to correspond to experimentally observed configurations, whereas unstable polymorphs above the hull could introduce inaccuracies and ambiguity when linking to experimental T_C values. In addition to the stability requirement we set, this limited availability of records arises also because the manually curated T_C dataset primarily includes disordered alloys, while the MP and AFLOW repositories focus on ordered structures.

For the classifier predicting the presence of an easy axis in a structure, we utilized the magnetic materials database from Sakurai et al. [28], which includes structures and MCA values for 3826 compounds. These mainly consist of TM elements, with Fe and Co as major constituents, due to their magnetic properties. This composition aligns with our study, as we primarily substitute Fe, Co, B, and N in the newly generated structures.

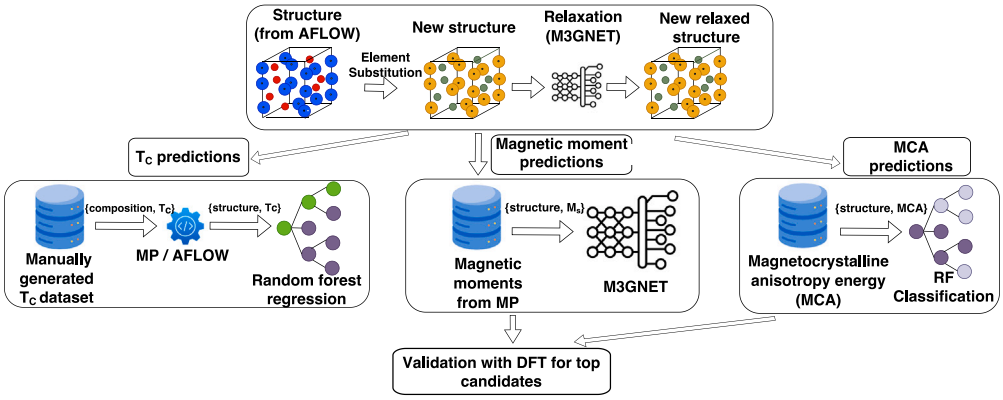

Fig. 1. Machine learning pipeline to discover new hard magnetic materials.

2.2. Training the machine learning models

M3GNet was used to train on the magnetic moment dataset comprising approximately 150,000 compounds. M3GNet is a graph-based deep-learning architecture, where the nodes represent the atoms and the edges the bonds of a crystal structure [23]. When trained on large datasets, graph-based networks outperform classical ML models that use simpler composition-based features [29,30]. The Adam optimizer [31] was used with an initial learning rate of 0.001, which decayed to 1% of its original value over 100 epochs using a cosine schedule. A batch size of 128 was used, with training completed in 750 epochs. The loss function employed was mean squared error (MSE).

For the T_C regressor and easy axis classifier, we utilized Matminer's structural feature generators along with a random forest (RF) model [32]. Each structure was used to generate features, including: (i) AGNIFingerprints, which integrate the radial distribution function and a Gaussian window function [33]; (ii) OPSiteFingerprint, representing local structural order parameters computed from a site's neighboring environment; and (iii) OrbitalFieldMatrix, which encodes the valence shell electron configurations of neighboring atoms. These combined features provided optimal performance on validation datasets for both the regressor and classifier. The RF models were implemented using scikit-learn [34] with 200 trees in the forest and a maximum depth of 20 for each tree.

2.3. Structure generation and relaxations

We began by downloading all ternary compounds composed of two TM elements and one non-TM element from the carbon group, boron group, pnictogens, or chalcogens using the AFLOW API [6]. This process yielded approximately 1.5 million structures, including experimentally derived and hypothetical structures. These were modified by substituting Fe and Co at the TM sites and B or N at the non-TM sites. For a generic composition TM^1_x-TM^2_y-nonTM$_z$, the following structures were generated: Fe_x-Co_y-N_z, Co_x-Fe_y-N_z, Fe_x-Co_y-B_z and Co_x-Fe_y-B_z. Duplicate structures were removed using Pymatgen's StructureMatcher algorithm [35], resulting in a dataset of approximately 48,000 unique structures. We note that this approach considers only one representative atomic configuration per stoichiometry. While multiple spatial arrangements may exist for a given composition, we have selected a single ordered configuration for computational efficiency. We believe this is a reasonable compromise that enables screening a broad design space, while recognizing that more exhaustive configurational sampling could be pursued in future work.

Before inference, these structures were relaxed using the M3GNet Interatomic Potential (IAP) graph network, trained on 187,000 energies, 16,000,000 forces, and 1,600,000 stresses from the Materials Project [23]. M3GNet was chosen for its efficiency in predicting structural properties, making it ideal for relaxing a dataset large enough to be impractical for DFT-based methods.

M3GNet extends CGCNN [36] graph-based representation by incorporating explicit three-body interactions, thereby capturing the multi-body correlation crucial for an accurate evaluation of the potential-energy surface and enabling both structural relaxations and molecular dynamics across diverse compositions. The focus on multi-body interactions and energy-force consistency grants M3GNet a high transferability and the flexibility to be applied to large-scale materials discovery. Adding to that, Xia et al. [17] introduced an adaptive genetic algorithm that refines its machine learning potential by iterating between candidate structure generation and targeted DFT validations, systematically improving accuracy when exploring high-anisotropy compounds. In our study, we do not utilize such an adaptive framework; instead, our approach leverages a large array of structural prototypes from the AFLOW repository to generate candidate structures, thus providing a broad sampling of compositions without iterative retraining.

2.4. DFT calculations

DFT calculations were performed using the projector augmented wave (PAW) method as implemented in the Vienna Ab-initio Simulation Package (VASP) [37]. The exchange–correlation functional was described using the generalized gradient approximation (GGA) in the Perdew, Burke, and Ernzerhof (PBE) form [38]. A kinetic-energy cutoff of 600 eV and the tetrahedron integration method [39] were employed. The convergence criteria were set to 10^{-7} eV for the total energy and 10^{-3} eV/Åfor the forces during ionic relaxation, with structural optimizations performed for both the cell volume and atomic positions.

The MCA was calculated using the magnetic force theorem [40–42]. This involved two steps: (i) a scalar-relativistic collinear charge self-consistent calculation to derive the charge density, followed by (ii) a non-self-consistent calculation, including spin–orbit coupling (SOC), to compute the total band energies for magnetization aligned parallel, $E_{\text{band},\parallel}$ and perpendicular, $E_{\text{band},\perp}$ to the crystal plane. The MCA was then determined as $E_{\text{MCA}} = E_{\text{band},\parallel} - E_{\text{band},\perp}$. This approach aligns well with prior studies on ferromagnetic systems [16,43].

The Monkhorst–Pack (MP) scheme was used to generate the **k**-point grid, ensuring convergence of the MCA energy to 10^{-6} eV/atom. Although MCA energies are small (typically on the order of meV), this approach reliably identifies anisotropic compounds.

At the lowest order the energy expression for the anisotropy of a magnet of volume V is determined by the K_1 anisotropy constant, through

$$E(\theta)/V = K_1 \sin^2\theta\,.$$

If $K_1 > 0$, then the energy has minima at $\theta = 0$ and $\theta = \pi$, which corresponds to easy-axis anisotropy. In the case of negative

K_1, the energy minimum occurs at $\theta = \pi/2$, where we have easy-plane anisotropy. However, the situation is different for low-symmetry crystal systems such as the orthorhombic, monoclinic and triclinic. In such cases, the anisotropy energy density up to second order can be expressed [44] as

$$E(\theta, \phi)/V = K_1 \sin^2\theta + K_1' \sin^2\theta \ \cos(2\phi)\,,$$

where K_1 and K_1' can be calculated from the energy differences between two interplanar and intraplanar magnetization directions [45].

In this study, K_1 was calculated using the first expression for all the 43 compounds as part of the primary screening. Due to computational limitations, the in-plane direction was restricted to [100] only. However, additional energy calculations have been performed along the [010] direction for a few most promising prototypes. Based on these results, the top five candidates have been selected. Our results are presented in Table 1. For the three lower-symmetry structures, both K_1 and K_1' are reported.

3. Results and discussions

3.1. Models predicting magnetic properties

We trained three separate machine learning models to predict key hard magnetic properties: M_S, T_C and easy axis anisotropy. The M3GNet graph network was trained on magnetic-moment data for 150,000 structures downloaded from the Materials Project. This dataset includes magnetic moments for materials in ferromagnetic, antiferromagnetic, ferrimagnetic and non-magnetic configurations. The model was trained for 750 epochs, with results for the training and validation datasets, as well as prediction plots for the test sets, shown in Fig. 2.

As shown in Fig. 2(a), the validation mean absolute error (MAE) of the magnetization model stabilizes around 0.15 $\mu_B/Å^3$. While this may appear large in absolute terms, it is important to recognize that the magnetization distribution is highly inhomogeneous, with most values clustered around zero and a long tail extending up to approximately 0.24 $\mu_B/Å^3$. As a reference, the magnetic polarization of elemental Fe and Co is estimated at 0.225 $\mu_B/Å^3$ and 0.146 $\mu_B/Å^3$, respectively, providing a useful context for interpreting the predicted values. For comparison, a trivial mean predictor achieves a MAE of 0.0201 $\mu_B/Å^3$, highlighting the challenge posed by this data distribution. Although restricting the training set to high-moment materials could reduce the prediction error, such an approach would bias the model toward overestimating magnetization. Our goal, instead, is to train a model that generalizes well across the full spectrum of magnetic behaviors. The so-constructed model achieves a R^2 score of 0.64 [see Fig. 2(b)], demonstrating its capability to capture meaningful trends and to distinguish between low- and high-moment candidates.

We also note that a related machine-learning model developed by Liao et al. [46] predicted total magnetic moment per unit cell in Fe-Co-N compounds with a root-mean-square error (RMSE) of 2.8 μ_B/cell. To compare this to our magnetization model, we converted their RMSE into an equivalent per-volume MAE using an average unit cell volume of 120 $Å^3$ for Fe-Co-N structures. This yields an estimated MAE of approximately 0.018 $\mu_B/Å^3$. While our reported MAE of 0.15 $\mu_B/Å^3$ is higher, the difference is expected due to our model's broader chemical scope, which includes both magnetic and non-magnetic materials.

Examining the prediction plot in Fig. 2(b), the graph networks clearly perform better when trained on properties such as formation energy, bulk modulus, or band gap [47], compared to the magnetic moment. Magnetic moments are highly sensitive to the choice of initial spin configurations, the presence of multiple competing magnetic states, and the limitations of standard exchange–correlation functionals in capturing electronic correlation effects. Furthermore, high-throughput DFT workflows often lack robust protocols for systematically determining the magnetic ground state [22], a feature that can lead to inconsistencies in the reported magnetic data. These factors contribute to greater uncertainty in the training data, and ultimately, lower model performance for the magnetic-moment prediction. Nonetheless, an R^2 of approximately 0.64 suggests that the model captures meaningful trends in the data and can help distinguish materials with relatively high magnetic moments. It is also worth noting that the machine learning models in this study are used primarily as a screening tool, with the final magnetic properties of selected candidates validated through direct DFT calculations.

Fig. 3 presents the parity plot for the T_C model computed over the test dataset. The model demonstrates the ability to predict T_C across its entire range, achieving a mean absolute error (MAE) of 75.6 K, which is comparable to the value of 57 K reported by Sanvito et al. [48]. Often T_C models underperform, particularly at high temperatures, due to the lack of training data in this range [48,49]. This limitation is common when models are trained using only compositional features. We further evaluated the model's performance in the high-T_C range and found that the MAE for compounds with $T_C > 300$ K is approximately 130 K. While this is higher than the overall MAE, it a result that reflects the greater spread of values at high temperatures. Despite this, the model still captures meaningful trends and remains useful for screening materials with high T_C.

Among the three models, predicting the MCA via regression proved to be the most challenging task. The difficulty stems from the lack of high-quality datasets, a fact that is linked to the computational complexity of calculating MCA values using DFT. As discussed in Section 2.1, we used the magnetic materials database from Ref. [17], which contains MCA values for approximately 3826 compounds along with their structures. We acknowledge that magnetocrystalline anisotropy (MCA) is a particularly difficult property to model using machine learning. This challenge stems not only from the inherent complexity of the MCA itself, which originates from subtle spin–orbit coupling effects, but also from the limitations of standard feature representations. The feature sets employed in this study, including composition-based fingerprints, local structural order parameters, and graph-based embeddings, do not explicitly capture critical physics such as crystal symmetry breaking, heavy-element orbital contributions, or spin–orbit–induced anisotropy. These limitations significantly hinder the model's ability to generalize across diverse material classes. Although the MCA data from Sakurai et al. [28] are of generally high quality and benchmarked against experimental values, the regression performance was ultimately constrained by descriptor sufficiency and model expressiveness. This suggests that future progress in MCA prediction will require incorporating symmetry and SOC aware descriptors tailored to the anisotropy problem, a direction we plan to explore in follow-up work.

In order to address these issues, we reformulated the problem as a classification task. Materials with negative MCA values were classified as easy plane and labeled as 0, while those with positive MCA were classified as easy axis and labeled as 1.

Fig. 4 shows the confusion matrix for the classifier. The model's performance, measured by the overall accuracy, was 0.66 on the test dataset. In a similar line of work, Xie et al. [50] developed an MCA classifier for 2D materials only for structures that are derived from changing the chemical composition of the ferromagnetic semiconductor $Cr_2Ge_2Te_6$, and achieved an accuracy of approximately 0.77. Given the diverse composition of our dataset, our model demonstrates sufficient predictive capabilities. As such, it serves as an effective screening tool to identify materials with a high likelihood of exhibiting easy axis anisotropy, providing a straightforward yet powerful filter for prioritizing candidates for further investigation.

It is important to note that all magnetocrystalline anisotropy (MCA) values reported in this study, both from DFT and ML, correspond to calculations performed at 0 K. No explicit temperature corrections were applied to the ML training data or the DFT-validated structures. As such, the reported K_1 values describe a ground-state property

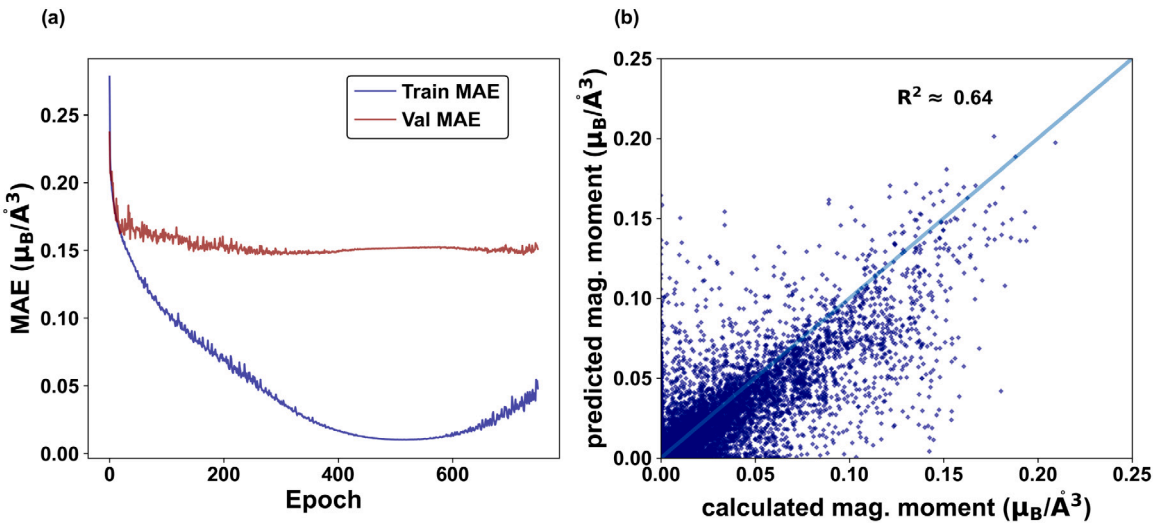

Fig. 2. Machine learning model used for magnetic moment prediction task: (a) Mean absolute error (MAE) of the magnetic moment per unit volume against the number of epochs, computed over the training and validation sets; (b) parity plots of the magnetic moment computed over the test dataset.

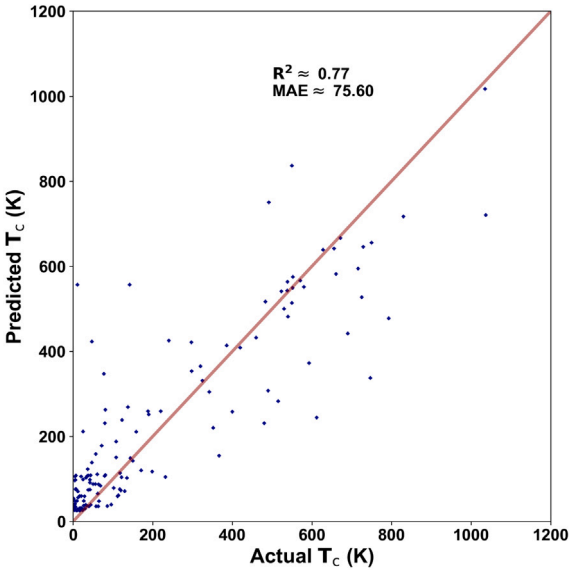

Fig. 3. Parity plot of the machine learning model for the T_C computed over the test dataset. Mean absolute error (MAE) and R^2 are provided in the legend.

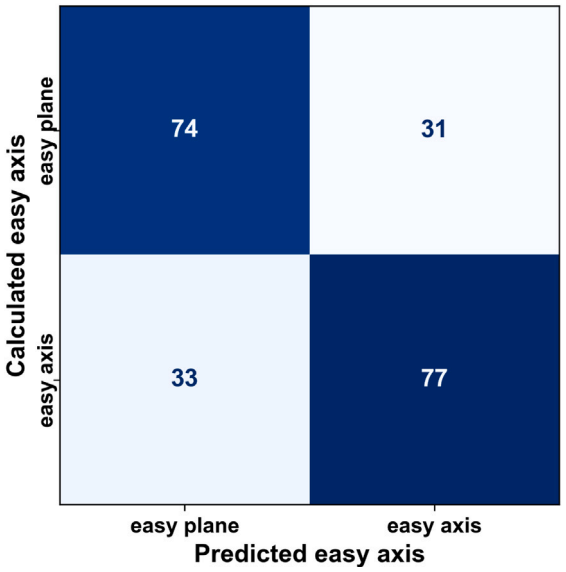

Fig. 4. Confusion matrix for the easy axis classifier model. The model predicts whether a material is likely to have easy plane or easy axis anisotropy, but does not provide an estimate for the magnetocrystalline anisotropy energy.

and may differ from those measured experimentally at finite temperatures. This limitation is inherent high-throughput DFT datasets incorporating MCA and is now acknowledged here for clarity. Incorporating temperature-dependent effects remains an important direction for future work.

3.2. M3GNet relaxation of new structures

When new structures are generated by substituting Fe, Co, B, and *N* into those obtained from AFLOW, both the atomic positions and lattice constants require optimization. DFT is the standard method for lattice relaxations; however, it is computationally demanding. Given the approximately 10,000 unique structures generated in this study, performing DFT relaxations on all of them is a large resource-consuming numerical task. In contrast, machine-learned interatomic potentials (IAPs) have demonstrated significant precision as surrogate models for property predictions, structural relaxations, and other tasks [23]. M3GNet, in particular, has been shown to relax arbitrary crystal structures at scale, making it an ideal choice for our materials discovery pipeline.

The M3GNet IAP was applied to these new structures, for which the final relaxed geometries were not known a priori. Fig. 5(a) and Fig. 6(a) show the cumulative distributions of volumes and energies of the crystal structures before and after M3GNet relaxation. The horizontal dashed lines mark the 50th, 80th, and 95th percentiles of the distributions (from bottom to top, respectively). Overall, the relaxation process leads to significant changes in both volume and energy, as expected. From the two figures, it is evident that more than 50% of the structures experienced volume changes greater than 35% and energy reductions exceeding 23%. Based on the energy lowering during relaxation, it is safe to state that M3GNet IAP was effective in relaxing the hypothetical crystals in a high-throughput manner. It is also worth mentioning that, while this served as an initial relaxation step, we performed further rigorous crystal optimizations for the top candidates

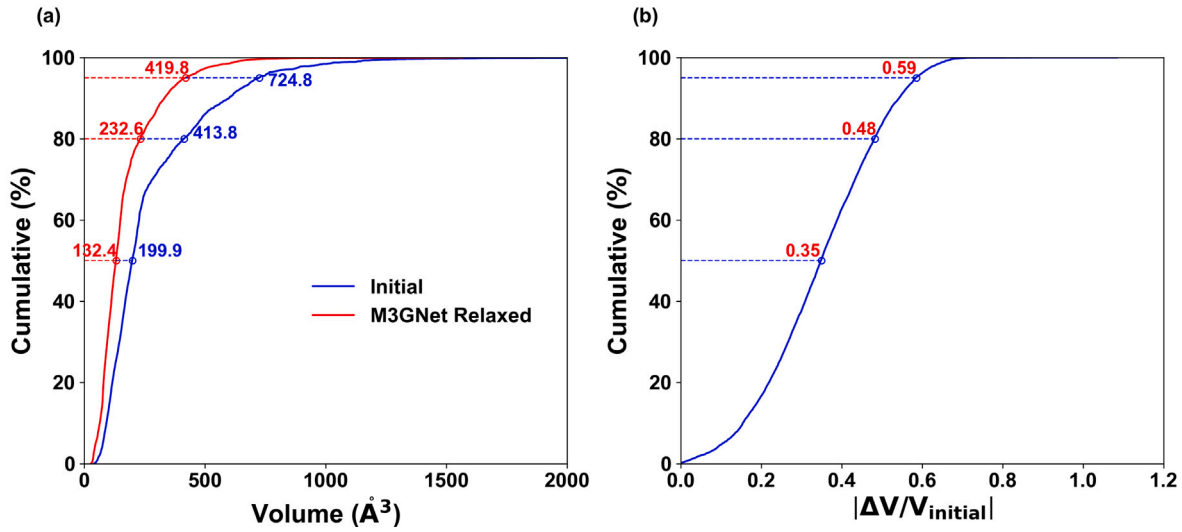

Fig. 5. Analysis of the M3GNet-driven crystal-structure relaxation: (a) Cumulative distribution of structure volumes before and after M3GNet relaxation; (b) differences between volumes before and after relaxation, relative to the initial volumes. Volumes refer to the total unit cell volumes of the structures before and after M3GNet relaxation.

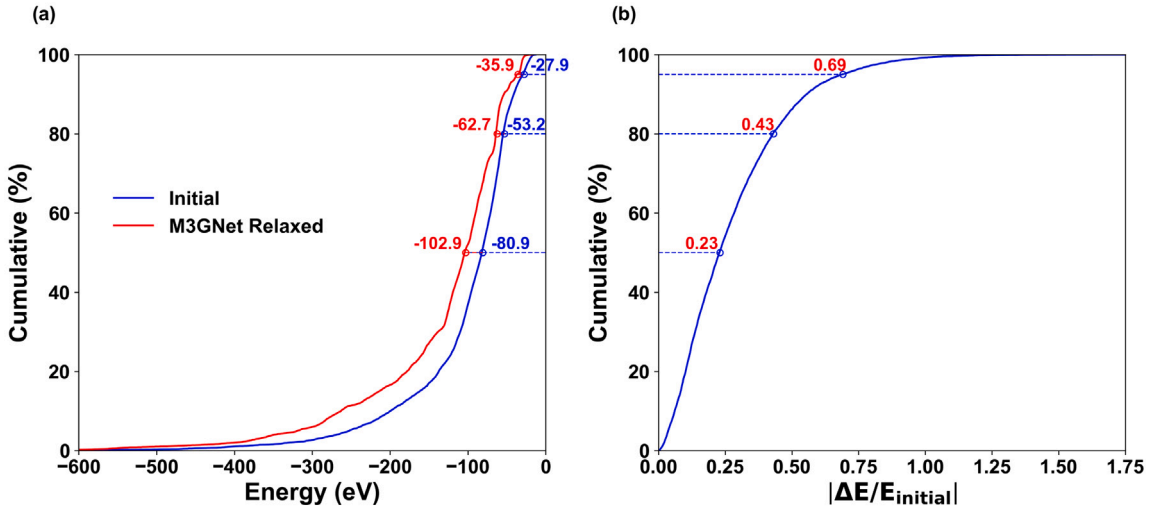

Fig. 6. Analysis of the M3GNet-driven crystal-structure relaxation: (a) Cumulative distribution of energies before and after M3GNet relaxation; (b) differences between energies before and after relaxation, relative to the initial energies. Energies represented are per unit cell.

during our DFT validation. To evaluate the accuracy of the M3GNet-relaxed geometries, we compared them to those obtained after full DFT optimization. As shown in Fig. 7, DFT refinement results in slightly smaller volumes, indicating that M3GNet provides a reasonable initial approximation that is further fine-tuned by DFT. The close clustering of points around the parity line confirms the overall consistency between the two relaxation methods. Lastly, we wish to remark that the M3GNet IAP relaxation does not provide information about thermodynamical stability. This requires further analyses, such as the prediction of the formation energy and the evaluation of the material's convex hull diagram. These aspects will be discussed in the next section.

3.3. Inference on the generated structures

The first step in assessing the thermodynamical stability of the generated structures involves predicting their formation energy. This is defined as the energy of the compound relative to the energies of its constituent elements in their lowest energy structure. A negative (positive) formation energy indicates that the compound is stable (unstable) against decomposition into its associated elemental phases. The formation energies of the hypothetical crystals generated in this study were predicted using the M3GNet graph network, which was trained on the Materials Project dataset with prediction errors below 30 meV/atom [47]. The distribution of formation energies is shown in Fig. 8, where it emerges that more than half of the structures are stable against elemental decomposition.

A more stringent stability assessment involves conducting a convex hull analysis, which compares the formation energy of a given compound to those of all known competing phases with the same composition. In particular, the analysis identifies the three nearest phases that form the vertices of the Gibbs triangle enclosing the compound's composition. PyMatGen [35] was used to perform this comparison against known structures in the Materials Project database. The energy above the hull is defined as the energy difference between the formation energy of a compound and the energy of the lowest-energy combination of competing phases at the same composition (most favorable decomposition). This value is denoted as E_{hull} and serves as a key thermodynamic stability metric. A compound with $E_{\text{hull}} = 0$ lies exactly on the convex hull and is predicted to be thermodynamically stable at zero temperature. Positive values of E_{hull} indicate metastability, with larger values implying a greater driving force toward decomposition. Compounds

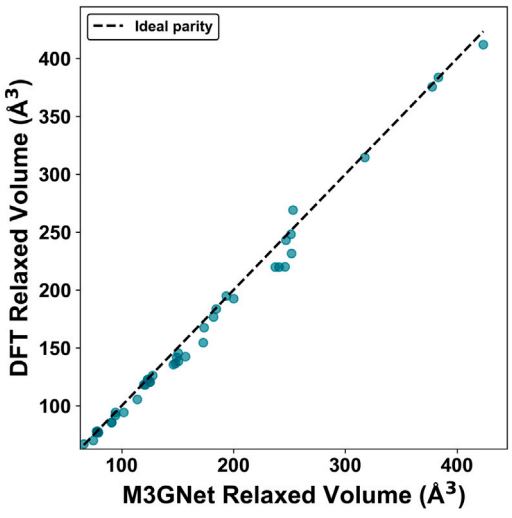

Fig. 7. Parity plot comparing the relaxed volumes obtained from M3GNet and full DFT optimization for the top candidate structures. The dashed line indicates perfect agreement.

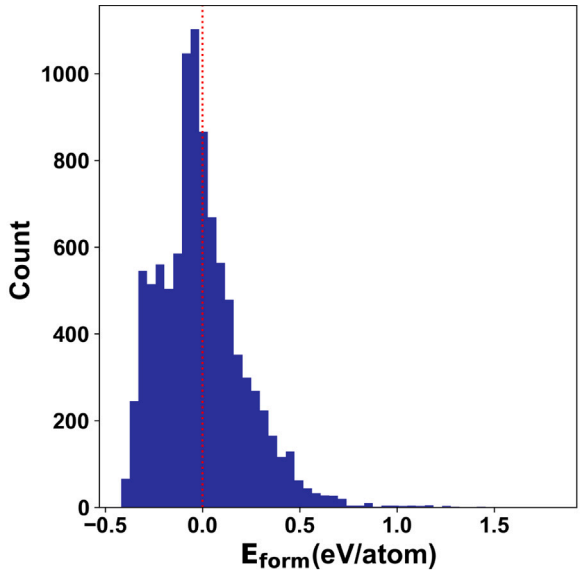

Fig. 8. Formation energy distribution predicted by M3GNet for the generated structures.

with E_{hull} less than 50–100 meV/atom are often regarded as potentially synthesizable, particularly under non-equilibrium synthesis conditions.

The results of such convex hull analyses are illustrated in Figs. 9(a) and 9(b) for the FeCoB- and FeCoN-type hypothetical structures, respectively. Although none of the hypothetical structures investigated here is below the tie plane of the convex hull, many structures lie close, with inverse hull energies smaller than 100 meV/atom. As a general guideline, materials with inverse hull energies below 100–300 meV/atom may be considered metastable [49]. Metastable structures can often be synthesized in experimentally by using non-equilibrium methods such as melt-spinning or ball milling [51].

The next stage in the materials discovery workflow uses ML models to predict key magnetic properties, namely M_S, T_C and easy axis MCA. Fig. 10 reports E_{hull} against M_S for the new structures, which satisfy our ML easy axis MCA screening, namely those structures that are likely to be easy axis anisotropic. Our goal is to identify new hard magnetic materials with large MCA, high M_S and high T_C. The stability criterion dictates that the formation energy of a compound must lie below or close to the convex hull. Therefore, we selected magnets with E_{hull} values less than 100 meV and M_S values greater than 1.34 T. This essentially corresponds to select potentially metastable structures with attractive magnetic performance. In addition, compounds with T_C above 600 K were filtered, as 600 K sets the boundary of magnets useful for every-day consumer applications. These criteria yielded 43 promising compounds, which were moved to further DFT validation.

3.4. Ab initio validation of the predicted structures

We now present our DFT results for the 43 compounds resulting from the ML screening. These comprise 37 FeCoB-type and 6 FeCoN-type structures. The calculated $\mu_0 M_S$ and K_1 values are shown in Fig. 11. Among these, 26 compounds exhibit $\mu_0 M_s > 1\ T$ (highlighted by the red-shaded area), while 18 have $K_1 > 0$ (blue-shaded area), indicating easy axis anisotropy. The agreement between the ML-predicted $\mu_0 M_S$ values and the DFT calculations is over 60%, slightly higher than the agreement obtained for K_1, which is at approximately 44%. Compounds meeting both criteria ($\mu_0 M_s > 1\ T$ and $K_1 > 0$) are considered potential candidates as hard magnets. There are 13 of them, as indicated by the overlap of the red and blue shaded areas in Fig. 11. These compounds clustered into 2–3 groups, with the largest group exhibiting high $\mu_0 M_S$ values and predominantly low K_1 values, along with a few moderate and 1–2 high K_1 values.

Although K_1 and $\mu_0 M_S$ provide valuable insights into a material's suitability as a permanent magnet, technologically relevant properties such as the maximum energy product, $(BH)_{max}$, and the anisotropy field, H_a, are more relevant. These can be calculated using K_1 and $\mu_0 M_s$ as follows

$$(BH)_{max} = \frac{(\mu_0 M_s)^2}{4\mu_0}, \quad H_a = \frac{2K_1}{\mu_0 M_s},$$

where $(BH)_{max}$ corresponds to the highest theoretical maximum, disregarding possible non-ideal hysteresis loop shapes.

In Fig. 12, we present $(BH)_{max}$ for all the compounds and H_a for most of them, excluding those with extremely small K_1 or $\mu_0 M_S$, resulting in a disproportionately large H_a. Compounds with $(BH)_{max} >$ 200 kJ/m^3 and $H_a > 1\ T$ are highlighted in the shaded regions. The computed $(BH)_{max}$ range in the 200–700 kJ/m^3 interval for more than 20 compounds, values comparable to commercially available hard-magnets, like $Nd_2Fe_{14}B$ (516 kJ/m^3) and $SmCo_5$ (219 kJ/m^3) [52]. Note, however, that our calculations overestimate $(BH)_{max}$ (possibly by about 10%), since bulk magnetic materials typically have hysteresis loop that deviate from an ideal shape, due to microstructuring, grain boundaries, etc. In contrast, the H_a ranges from −4 T to 4 T, with at least 10 compounds exhibiting $H_a > 1$ T, highlighting their potential for easy axis anisotropy.

Another important metric for classifying magnets as hard, semi-hard, or soft is the hardness parameter, κ, which is calculated as

$$\kappa = \sqrt{\frac{K_1}{\mu_0 M_s^2}}.$$

A magnet is hard if $\kappa > 1$. Our calculations identified 5–6 compounds with $\kappa \approx 1$, indicating their potential for hard magnet applications.

The top five candidates were selected based on the criteria $\mu_0 M_s > 1$ T and $K_1 > 0$. Key magnetic properties, including K_1, $\mu_0 M_S$, $(BH)_{max}$, κ, as well as the convex hull energy, E_{hull}, and the formation energy, E_{form}, are listed in Table 1, together with their corresponding crystal space group symmetries, as shown in Fig. 13. All compounds are stable against decomposition into their constituent elements, as E_{form} is negative for all of them. Among the listed compounds, Fe_6CoB_2 exhibits the highest K_1, 1.763 MJ/m^3, combined with a substantial $\mu_0 M_S$ of 1.736 T, leading to a high $(BH)_{max}$, namely 600.175 kJ/m^3. This compound also shows a relatively low energy above the convex

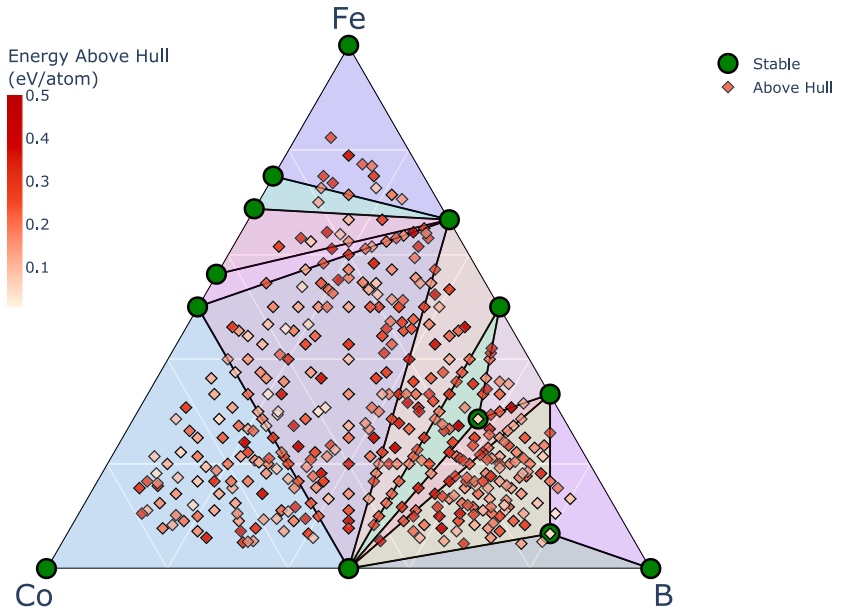

(a) FeCoB ternary

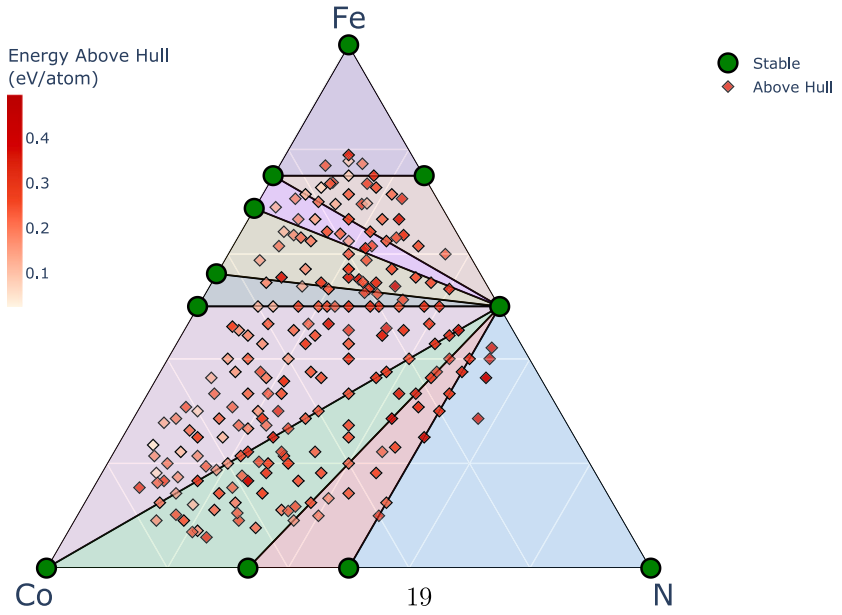

(b) FeCoN ternary

Fig. 9. Convex hull analyses for the (a) FeCoB and (b) FeCoN ternary compounds investigated in this study.

Table 1
DFT-calculated formation energies and intrinsic magnetic properties of the top permanent-magnet candidates. The structures are shown in Fig. 13. Estimates of T_C and E_{hull} are provided with the ML model.

Compound	Crystal symmetry	E_{hull} (meV/atom)	E_{form} (meV/atom)	$K_1(K_1')$ (MJ/m^3)	BH_{max} (kJ/m^3)	$\mu_0 M_S$ (T)	μ_B/fu	κ	T_C (K)
$FeCo_5B$	Tetragonal	68.521	−170.251	1.001 (–)	376.249	1.374	8.279	0.816	785
$Fe_{10}CoB_3$	Trigonal	96.553	−71.708	0.559 (–)	633.376	1.783	21.029	0.470	681
Fe_6CoB_2	Monoclinic	30.431	−215.781	1.763 (0.608)	600.175	1.736	12.783	0.857	624
Fe_4CoB	Orthorhombic	78.296	−154.807	0.598 (0.383)	688.377	1.860	10.069	0.466	605
Fe_2Co_6N	Monoclinic	90.031	−38.248	0.223 (−0.036)	507.428	1.596	12.594	0.332	666

hull, E_{hull} = 30.4 meV/atom, indicating the possibility of metastabilty. The second notable candidate is $FeCo_5B$, with K_1 = 1.001 MJ/m^3, $(BH)_{max}$ = 376.248 kJ/m^3, and E_{hull} = 68.5 meV/atom. In the case of $Fe_{10}CoB_3$, a moderate K_1 of 0.559 MJ/m^3 is combined with a high $(BH)_{max}$ of 633.376 kJ/m^3 and E_{hull} = 96.5 meV/atom. A similar situation is observed for Fe_4CoB, which combines a moderate K_1 of 0.598 MJ/m^3 with the highest $(BH)_{max}$ of 688.377 kJ/m^3 and $\mu_0 M_S$ of 1.860 T. The only nitride-based compound in the list is Fe_2Co_6N, which

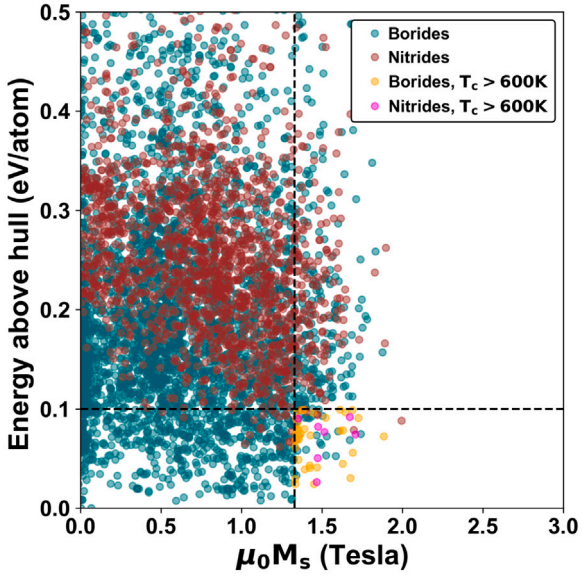

Fig. 10. Distribution of potential hard-magnet candidates. The plot presents the distribution of compounds against their energy above the convex hull, E_{hull}, and saturation magnetization, M_S. The top candidates according to their thermodynamic stability, saturation magnetization and with a Curie temperature ≥ 600 K are colored in yellow (borides) and pink (nitrides) in the bottom-right quadrant. These structure, 43 in total, were further analyzed by density functional theory.

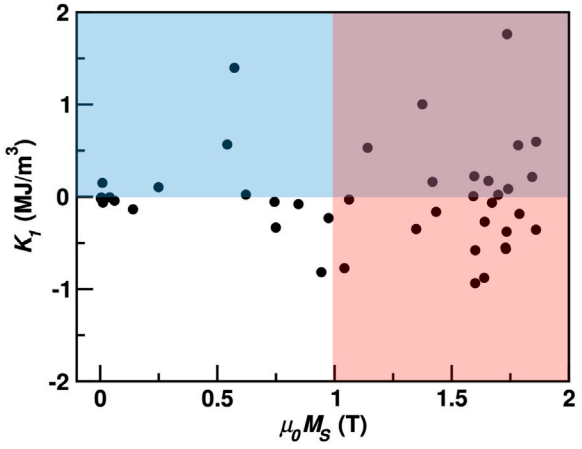

Fig. 11. The density functional theory-calculated anisotropy constant, K_1, and saturation magnetization $\mu_0 M_S$ are presented for all compounds. Positive (negative) values of K_1 indicate an easy axis (easy plane) preference for the magnetization. The blue-shaded area highlights compounds with easy axis anisotropy, while the red-shaded area indicates compounds with $\mu_0 M_S$ greater than 1 T.

shows a substantial $(BH)_{\text{max}}$ of 507.428 kJ/m^3 and $\mu_0 M_S$ of 1.596 T, although K_1 = 0.223 MJ/m^3 is relatively low compared to the other four compounds.

In this context, it is worth mentioning that the orbital magnetic moments of these compounds is primarily determined by the Co and Fe atoms. The magnitude for Co (0.03–0.1 μ_B) is slightly larger than that for Fe (0.009–0.063 μ_B). The difference in the total orbital moment between the two magnetization directions is related to the MCA, which is consistent with the perturbative expression of the MCA energy as shown by Bruno [53].

In Xia et al. [17], several Fe-Co-B compounds were reported displaying strong intrinsic magnetic properties. Fe_3CoB_2 stands out with K_1 = 1.34 MJ/m^3, J_s = 1.40 T, and a low E_{hull} = 22.8 meV/atom, a compound that was also experimentally synthesized. Based on the space group information (Cmmm) provided by Xia et al. [17], we

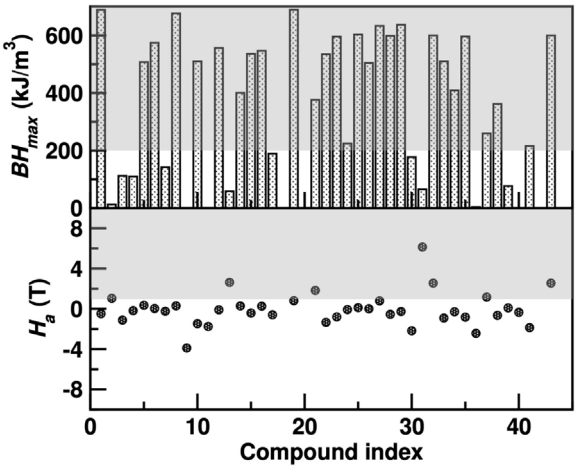

Fig. 12. Calculated maximum theoretical energy product, $(BH)_{\text{max}}$ (upper panel) and anisotropy field, H_a (lower panel) for all the screened compounds. The shaded regions highlight compounds with $(BH)_{\text{max}}$ > 200 kJ/m^3 and H_a > 1 T.

confirm that the Fe_3CoB_2 compound is indeed present in our generated database. Its computed properties are: $\mu_0 M_S$ = 0.97 T, and T_C = 508 K, with an energy above hull (E_{hull}) of 0.29 eV/atom. Despite having respectable magnetic performance, this compound did not pass our high-throughput filtering criteria, which included thresholds of T_C > 600 K, $\mu_0 M_S$ > 1.33 T, and E_{hull} < 0.1 eV/atom. Therefore, it was not selected for DFT validation in the final round. We note that although the compound appears in both studies under the same nominal composition, differences in the specific Wyckoff site occupations and structural relaxations may lead to variations in the predicted properties.

Other high-anisotropy compounds, such as certain Fe_2CoB_2 polymorphs, exhibit K_1 values approaching 1.96 MJ/m^3 but with higher E_{hull} values exceeding 90 meV/atom. One of our prime candidates, monoclinic Fe_6CoB_2, delivers K_1 = 1.76 MJ m^{-3}, $\mu_0 M_s$ = 1.74 T and E_{hull} = 30.4 meV atom^{-1}. Although the two compounds are crystallographically distinct, their similar compositions yield comparable energetics and magnetic performance, lending confidence to the predictions. In addition, the fact that this compound was experimentally realized while having E_{hull} = 22.8 meV/atom is promising, as Fe_6CoB_2, shows a comparable E_{hull} of 30.4 meV/atom, indicating that it may also be experimentally accessible.

Our tetragonal $FeCo_5B$ and orthorhombic Fe_4CoB can be compared with the well-documented tetragonal $(Fe_{1-x}Co_x)_2B$ series. For composition at $x \approx 0.3$ Edström et al. [11] reported K_1 = 0.42-0.63 MJ m^{-3} and $T_C \approx$ 800-820 K, while our prediction range for these compounds is K_1 = 0.60-1.00 MJ m^{-3} (see Table 1), hence corroborating the ML-DFT pipeline.

Nitrides hard-magnet remain scarce. The reference thin-film phase α''-$Fe_{16}N_2$ reaches up $K_u \approx$ 0.6 MJ m^{-3} [54], whereas theory yields K_u = 3.2 MJ m^{-3} for $Fe_{12}Co_4N_2$ [55]. We find that monoclinic Fe_2CoN_6 has K_1 = 0.22 MJ m^{-3} and $\mu_0 M_s$ = 1.60 T, values consistent with these predictions. In addition, existing Fe-Co-N sputtered films are magnetically soft in spite of their high M_s [56], a fact that aligns with our low K_1 prediction for these compounds.

Thus, taken all together, these comparisons show that the present workflow (i) faithfully reproduces the intrinsic properties of experimentally established magnets in the Fe-Co-B and Fe-Co-N systems and (ii) uncovers several genuinely new, metastable boride and nitride phases that are well within reach of modern rapid-quenching or thin-film synthesis techniques.

For reproducibility, the CIF files of the top candidate structures have been included as supplementary materials. These provide full crystallographic information, including lattice parameters, atomic positions, and species ordering, to facilitate verification and further analysis.

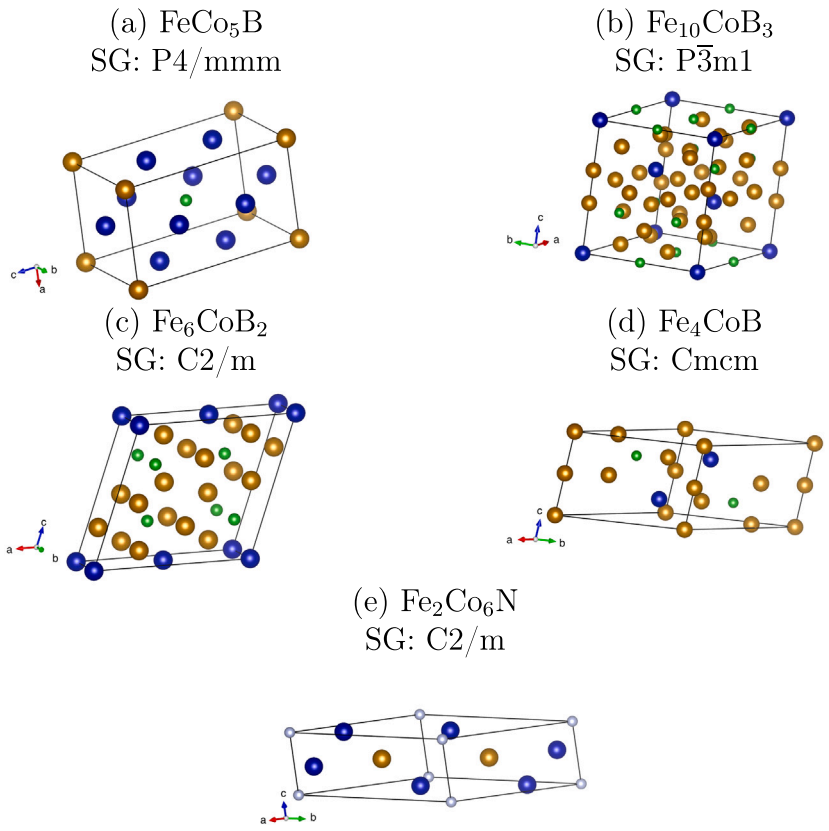

Fig. 13. Crystal structure diagrams (primitive unit cell) of the most promising hard magnets with the associated space groups (SG). Their computed magnetic properties are listed in Table 1. Fe, Co, B ad *N* atoms are represented by gold, blue, green and gray spheres respectively.

4. Conclusions

This study presents a robust high-throughput framework combining machine learning (ML) and density functional theory (DFT) to streamline the discovery of high-performance hard magnetic materials. By leveraging advanced ML models, structural relaxation using M3GNet, and high-throughput DFT validation, this approach efficiently identifies FeCo-based ternary alloys with exceptional magnetic properties, including uniaxial anisotropy, saturation magnetization, and Curie temperature. For example, Fe_6CoB_2 demonstrates superior performance with a uniaxial anisotropy constant (K_1) of 1.763 MJ/m^3, saturation magnetization (M_S) of 1.736 T, and Curie temperature (T_C) of 624 K. Similarly, $FeCo_5B$ exhibits K_1 = 1.001 MJ/m^3, M_S = 1.374 T, and T_C = 785 K, while Fe_4CoB achieves K_1 = 0.598 MJ/m^3, M_S = 1.860 T, and T_C = 605 K, making them strong candidates for high-performance magnetic applications. Note that all these are not on the convex hull, but they are sufficiently close to be considered metastable.

The integration of ML models for rapid screening and predictive accuracy underscores the potential of data-driven methodologies to overcome the limitations of traditional trial-and-error approaches to materials discovery. This study not only highlights the feasibility of accelerating materials discovery, but also provides a scalable and adaptable workflow for exploring other magnetic systems. Future efforts will focus on refining predictive models, expanding the dataset, and applying this pipeline to a broader range of material compositions.

CRediT authorship contribution statement

Anita Halder: Writing – original draft, Methodology, Formal analysis. **Durga Paudyal:** Writing – review & editing. **Stefano Sanvito:** Writing – review & editing, Resources. **Martin Takáč:** Writing – review & editing, Resources, Methodology. **Huseyin Ucar:** Writing – original draft, Supervision, Conceptualization.

Data and software availability

The source code developed for training machine learning models, along with the code for retrieving ternaries from aflow.org, substitutions performed to generate new alloys are available at https://github.com/ucarh/ML_driven_PM_discovery for reproducibility.

Declaration of competing interest

The authors declare that they have no known competing financial interests or personal relationships that could have appeared to influence the work reported in this paper.

Acknowledgments

H.U. gratefully acknowledges financial support for this research by the Fulbright U.S. Scholar Program, which is sponsored by the U.S. Department of State, United States. A.H. was supported by European Commission through the Marie Skłodowska-Curie individual fellowship VOLTEMAG-101065605. The work of D. P. at University of Iowa was supported as part of the Center for Energy Efficient Magnonics, an Energy Frontier Research Center funded by the U.S. Department of Energy, United States, Office of Science, Basic Energy Sciences, under Award number DE-AC02-76SF00515. S.S. acknowledge funding from Research Ireland: AMBER Research Center (12/RC/2278_P2) and Advanced Laureate Award (IRCLA/2019/127). The authors thank Aigerim Zhumabayeva for her invaluable assistance and insightful discussions throughout this research.

Appendix A. Supplementary data

Supplementary material related to this article can be found online at https://doi.org/10.1016/j.actamat.2025.121347.

References

[1] M. Kramer, R. McCallum, I. Anderson, S. Constantinides, Prospects for non-rare earth permanent magnets for traction motors and generators, JOM 64 (2012) 752–763.

[2] H. Ucar, D. Paudyal, K. Choudhary, Machine learning predicted magnetic entropy change using chemical descriptors across a large compositional landscape, Comput. Mater. Sci. 209 (2022) 111414.

[3] J. Coey, Magnetism and Magnetic Materials, second ed., Cambridge University Press, 2025.

[4] S. Curtarolo, G.L.W. Hart, M.B. Nardelli, N. Mingo, S. Sanvito, O. Levy, The high-throughput highway to computational materials design, Nat. Mater. 12 (2013) 191–201.

[5] S. Kirklin, J.E. Saal, B. Meredig, A. Thompson, J.W. Doak, M. Aykol, S. Rühl, C. Wolverton, The Open Quantum Materials Database (OQMD): assessing the accuracy of DFT formation energies, NPJ Comput. Mater. 1 (1) (2015) 1–15.

[6] S. Curtarolo, W. Setyawan, S. Wang, J. Xue, K. Yang, R.H. Taylor, L.J. Nelson, G.L. Hart, S. Sanvito, M. Buongiorno-Nardelli, et al., AFLOWLIB. ORG: A distributed materials properties repository from high-throughput ab initio calculations, Comput. Mater. Sci. 58 (2012) 227–235.

[7] A. Jain, S.P. Ong, G. Hautier, W. Chen, W.D. Richards, S. Dacek, S. Cholia, D. Gunter, D. Skinner, G. Ceder, et al., Commentary: The materials project: A materials genome approach to accelerating materials innovation, APL Mater. 1 (1) (2013).

[8] J.-X. Zhu, M. Janoschek, R. Rosenberg, F. Ronning, J.D. Thompson, M.A. Torrez, E.D. Bauer, C.D. Batista, LDA+ DMFT approach to magnetocrystalline anisotropy of strong magnets, Phys. Rev. X 4 (2) (2014) 021027.

[9] B. Ensign, R. Choudhary, H. Ucar, D. Paudyal, Electronic structure, magnetic properties, and exchange splitting of gadolinium intermetallics, J. Magn. Magn. Mater. 509 (2020) 166882.

[10] H. Ucar, R. Choudhary, D. Paudyal, Substitutional and interstitial doping in $LaCo_5$ system for the development of hard magnetic properties: A first principles study, J. Alloys Compd. 836 (2020) 155263.

[11] A. Edström, J. Chico, A. Jakobsson, A. Bergman, J. Rusz, Electronic structure and magnetic properties of $L1_0$ binary alloys, Phys. Rev. B 90 (1) (2014) 014402.

[12] A. Liechtenstein, V.I. Anisimov, J. Zaanen, Density-functional theory and strong interactions: Orbital ordering in Mott-Hubbard insulators, Phys. Rev. B 52 (8) (1995) R5467.

[13] G.R. Schleder, A.C. Padilha, C.M. Acosta, M. Costa, A. Fazzio, From DFT to machine learning: recent approaches to materials science–a review, J. Phys.: Mater. 2 (3) (2019) 032001.

[14] O. Grånäs, I. Di Marco, P. Thunström, L. Nordström, O. Eriksson, T. Björkman, J. Wills, Charge self-consistent dynamical mean-field theory based on the full-potential linear muffin-tin orbital method: Methodology and applications, Comput. Mater. Sci. 55 (2012) 295–302.

[15] S. Sanvito, C. Oses, J. Xue, A. Tiwari, M. Zic, T. Archer, P. Tozman, M. Venkatesan, M. Coey, S. Curtarolo, Accelerated discovery of new magnets in the Heusler alloy family, Sci. Adv. 3 (4) (2017) e1602241.

[16] A. Halder, S. Rom, A. Ghosh, T. Saha-Dasgupta, Prediction of the properties of the rare-earth magnets $Ce_2Fe_{17-x}Co_xCN$: A combined machine-learning and ab initio study, Phys. Rev. Appl. 14 (2020) 034024, http://dx.doi.org/10.1103/PhysRevApplied.14.034024, URL https://link.aps.org/doi/10.1103/PhysRevApplied.14.034024.

[17] W. Xia, M. Sakurai, B. Balasubramanian, T. Liao, R. Wang, C. Zhang, H. Sun, K.-M. Ho, J.R. Chelikowsky, D.J. Sellmyer, et al., Accelerating the discovery of novel magnetic materials using machine learning–guided adaptive feedback, Proc. Natl. Acad. Sci. 119 (47) (2022) e2204485119.

[18] W. Xia, M. Sakurai, T. Liao, R. Wang, C. Zhang, H. Sun, K.-M. Ho, J.R. Chelikowsky, C.-Z. Wang, Machine learning assisted search for Fe–Co–C ternary compounds with high magnetic anisotropy, APL Mach. Learn. 2 (4) (2024).

[19] T. Liao, W. Xia, M. Sakurai, C. Zhang, H. Sun, R. Wang, K.-M. Ho, C.-Z. Wang, J.R. Chelikowsky, Machine learning-accelerated discovery of iron cobalt phosphides as rare-earth-free magnets, Phys. Rev. Mater. 8 (10) (2024) 104404.

[20] J. Schmidt, L. Pettersson, C. Verdozzi, S. Botti, M.A. Marques, Crystal graph attention networks for the prediction of stable materials, Sci. Adv. 7 (49) (2021) eabi7948.

[21] A. Vishina, D. Hedlund, V. Shtender, E.K. Delczeg-Czirjak, S.R. Larsen, O.Y. Vekilova, S. Huang, L. Vitos, P. Svedlindh, M. Sahlberg, et al., Data-driven design of a new class of rare-earth free permanent magnets, Acta Mater. 212 (2021) 116913.

[22] M.K. Horton, J.H. Montoya, M. Liu, K.A. Persson, High-throughput prediction of the ground-state collinear magnetic order of inorganic materials using density functional theory, NPJ Comput. Mater. 5 (1) (2019) 64.

[23] C. Chen, S.P. Ong, A universal graph deep learning interatomic potential for the periodic table, Nat. Comput. Sci. 2 (11) (2022) 718–728.

[24] H. Ucar, R. Choudhary, D. Paudyal, An overview of the first principles studies of doped RE-TM5 systems for the development of hard magnetic properties, J. Magn. Magn. Mater. 496 (2020) 165902.

[25] J. Coey, Hard magnetic materials: A perspective, IEEE Trans. Magn. 47 (12) (2011) 4671–4681.

[26] A. Zhumabayeva, N. Ranjan, M. Takáč, S. Sanvito, H. Ucar, MagBERT: Magnetics knowledge aware language model coupled with a question answering pipeline for curie temperature extraction task, J. Phys. Chem. C 128 (31) (2024) 13217–13229.

[27] L.P. Gilligan, M. Cobelli, V. Taufour, S. Sanvito, A rule-free workflow for the automated generation of databases from scientific literature, NPJ Comput. Mater. 9 (1) (2023) 222.

[28] M. Sakurai, R. Wang, T. Liao, C. Zhang, H. Sun, Y. Sun, H. Wang, X. Zhao, S. Wang, B. Balasubramanian, et al., Discovering rare-earth-free magnetic materials through the development of a database, Phys. Rev. Mater. 4 (11) (2020) 114408.

[29] S. Kearnes, K. McCloskey, M. Berndl, V. Pande, P. Riley, Molecular graph convolutions: moving beyond fingerprints, J. Comput. Aided Mol. Des. 30 (2016) 595–608.

[30] Y. Li, D. Tarlow, M. Brockschmidt, R. Zemel, Gated graph sequence neural networks, 2015, arXiv preprint arXiv:1511.05493.

[31] D.P. Kingma, Adam: A method for stochastic optimization, 2014, arXiv preprint arXiv:1412.6980.

[32] L. Breiman, Random forests, Mach. Learn. 45 (2001) 5–32.

[33] V. Botu, R. Batra, J. Chapman, R. Ramprasad, Machine learning force fields: construction, validation, and outlook, J. Phys. Chem. C 121 (1) (2017) 511–522.

[34] F. Pedregosa, Scikit-learn: Machine learning in python Fabian, J. Mach. Learn. Res. 12 (2011) 2825.

[35] S.P. Ong, W.D. Richards, A. Jain, G. Hautier, M. Kocher, S. Cholia, D. Gunter, V.L. Chevrier, K.A. Persson, G. Ceder, Python materials genomics (pymatgen): A robust, open-source python library for materials analysis, Comput. Mater. Sci. 68 (2013) 314–319.

[36] T. Xie, J.C. Grossman, Crystal graph convolutional neural networks for an accurate and interpretable prediction of material properties, Phys. Rev. Lett. 120 (14) (2018) 145301.

[37] G. Kresse, J. Hafner, Ab initio molecular dynamics for liquid metals, Phys. Rev. B 47 (1993) 558–561, http://dx.doi.org/10.1103/PhysRevB.47.558, URL https://link.aps.org/doi/10.1103/PhysRevB.47.558.

[38] J.P. Perdew, K. Burke, M. Ernzerhof, Generalized gradient approximation made simple, Phys. Rev. Lett. 77 (1996) 3865–3868, http://dx.doi.org/10.1103/PhysRevLett.77.3865, URL https://link.aps.org/doi/10.1103/PhysRevLett.77.3865.

[39] P.E. Blöchl, O. Jepsen, O.K. Andersen, Improved tetrahedron method for brillouin-zone integrations, Phys. Rev. B 49 (1994) 16223–16233, http://dx.doi.org/10.1103/PhysRevB.49.16223, URL https://link.aps.org/doi/10.1103/PhysRevB.49.16223.

[40] O.K. Andersen, H.L. Skriver, H. Nohl, J. B., Pure Appl. Chem. 52 (1979) 93.

[41] M. Weinert, R.E. Watson, J.W. Davenport, Total-energy differences and eigenvalue sums, Phys. Rev. B 32 (1985) 2115–2119, http://dx.doi.org/10.1103/PhysRevB.32.2115, URL https://link.aps.org/doi/10.1103/PhysRevB.32.2115.

[42] G.H.O. Daalderop, P.J. Kelly, M.F.H. Schuurmans, First-principles calculation of the magnetocrystalline anisotropy energy of iron, cobalt, and nickel, Phys. Rev. B 41 (1990) 11919–11937, http://dx.doi.org/10.1103/PhysRevB.41.11919, URL https://link.aps.org/doi/10.1103/PhysRevB.41.11919.

[43] A. Halder, S. Bhandary, D.D. O'Regan, S. Sanvito, A. Droghetti, Theoretical perspective on the modification of the magnetocrystalline anisotropy at molecule-cobalt interfaces, Phys. Rev. Mater. 7 (2023) 064409, http://dx.doi.org/10.1103/PhysRevMaterials.7.064409, URL https://link.aps.org/doi/10.1103/PhysRevMaterials.7.064409.

[44] R. Skomski, Simple Models of Magnetism, Oxford University Press, 2008, http://dx.doi.org/10.1093/acprof:oso/9780198570752.001.0001.

[45] I. Ahamed, R. Pathak, R. Skomski, A. Kashyap, Magnetocrystalline anisotropy of ϵ-Fe_2O_3.

[46] T. Liao, et al., Large magnetic anisotropy predicted for rare-earth-free $Fe_{16-x}Co_xN_2$ alloys, Phys. Rev. Mater. 6 (2) (2022) 024402, http://dx.doi.org/10.1103/PhysRevMaterials.6.024402.

[47] C. Chen, W. Ye, Y. Zuo, C. Zheng, S.P. Ong, Graph networks as a universal machine learning framework for molecules and crystals, Chem. Mater. 31 (9) (2019) 3564–3572.

[48] J.F. Belot, V. Taufour, S. Sanvito, G.L. Hart, Machine learning predictions of high-curie-temperature materials, Appl. Phys. Lett. 123 (4) (2023).

[49] C.J. Court, A. Jain, J.M. Cole, Inverse design of materials that exhibit the magnetocaloric effect by text-mining of the scientific literature and generative deep learning, Chem. Mater. 33 (18) (2021) 7217–7231.

[50] Y. Xie, G.A. Tritsaris, O. Granas, T.D. Rhone, Data-driven studies of the magnetic anisotropy of two-dimensional magnetic materials, J. Phys. Chem. Lett. 12 (50) (2021) 12048–12054.

[51] M.E. McHenry, M.A. Willard, D.E. Laughlin, Amorphous and nanocrystalline materials for applications as soft magnets, Prog. Mater. Sci. 44 (4) (1999) 291–433.

[52] K.J. Buschow, Concise Encyclopedia of Magnetic and Superconducting Materials, Elsevier, 2005.

[53] P. Bruno, Tight-binding approach to the orbital magnetic moment and magnetocrystalline anisotropy of transition-metal monolayers, Phys. Rev. B 39 (1989) 865–868, http://dx.doi.org/10.1103/PhysRevB.39.865, URL https://link.aps.org/doi/10.1103/PhysRevB.39.865.

[54] J. Coey, New permanent magnets; manganese compounds, J. Phys.: Condens. Matter. 26 (6) (2014) 064211.
[55] X. Zhao, C.-Z. Wang, Y. Yao, K.-M. Ho, Large magnetic anisotropy predicted for rare-earth-free $Fe_{16-x}Co_xn_2$ alloys, Phys. Rev. B 94 (22) (2016) 224424.
[56] Z. Han, C. Song, J. Zhou, Z. Ma, L. Ma, H. Gao, F. Zheng, Influence of the deposition conditions on the magnetic properties of Fe–Co–N thin films, J. Alloys Compd. 934 (2023) 167951.